Electronic Supplementary Information

Impregnating ultrafine FeS_2 nanoparticles within hierarchical carbon tubes for advanced potassium-ion batteries

Zhuangzhuang Zhang[a], Yaru Qiao[a], Qinghua Deng[b], Mengmin Jia[a], Dai-Huo Liu[a]*, Dongmei Dai[a]* and Bao Li[a]*

[a] Collaborative Innovation Center of Henan Province for Green Manufacturing of Fine Chemicals, Key Laboratory of Green Chemical Media and Reactions, Ministry of Education, School of Chemistry and Chemical Engineering, Henan Normal University, Xinxiang, Henan 453007, China.

Corresponding Authors: *E-mail: libao@htu.edu.cn, daidongmei@htu.edu.cn, liudaihuo@htu.edu.cn

[b] School of Chemistry and Chemical Engineering, Southeast University, Nanjing 211189, China

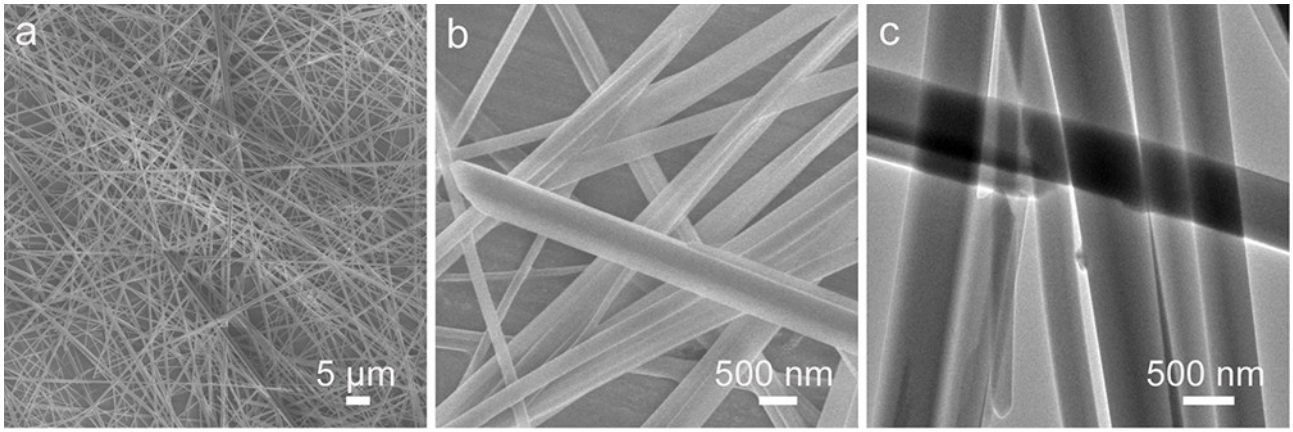

Fig. S1. (a, b) SEM images and (c) TEM images of Fe-NTAC nanowires.

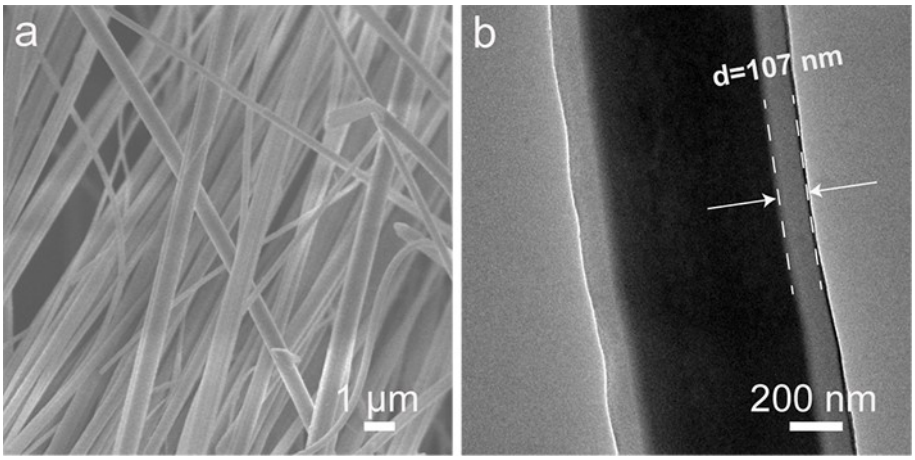

Fig. S2. (a) SEM image and (b) TEM image of Fe-NTAC@GC nanowires.

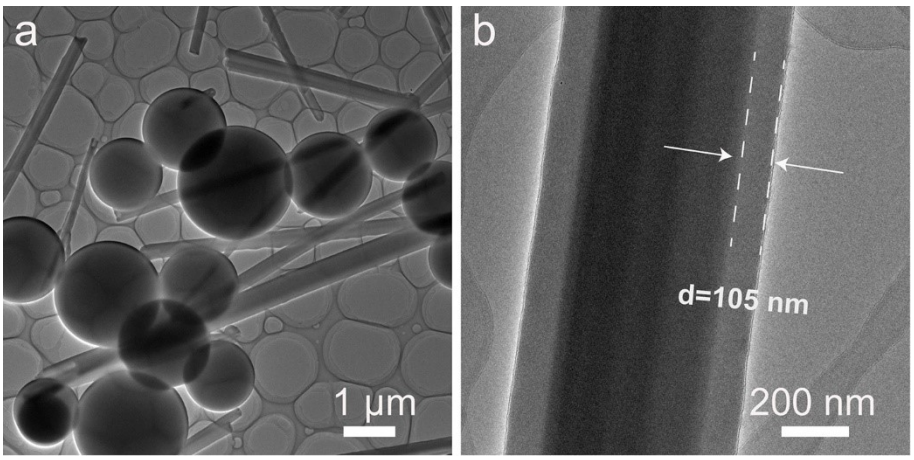

Fig. S3. (a) and (b) TEM images of Fe-NTAC@GC nanowires prepared by suing 1.5 g of glucose.

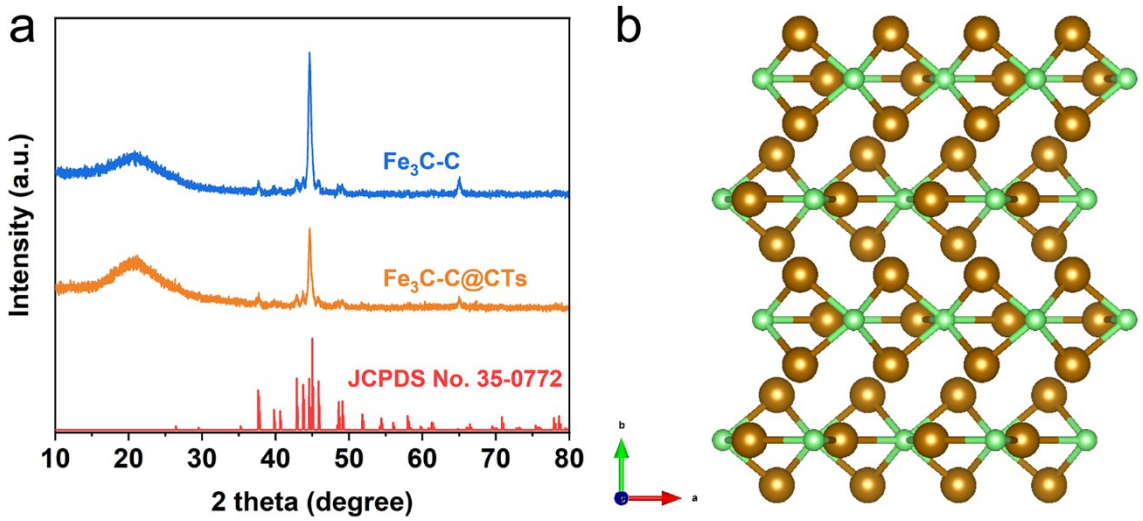

Fig. S4. (a) XRD pattern of Fe_3C@C and Fe_3C-C@CTs nanowires, and (b) crystal structure of Fe_3C.

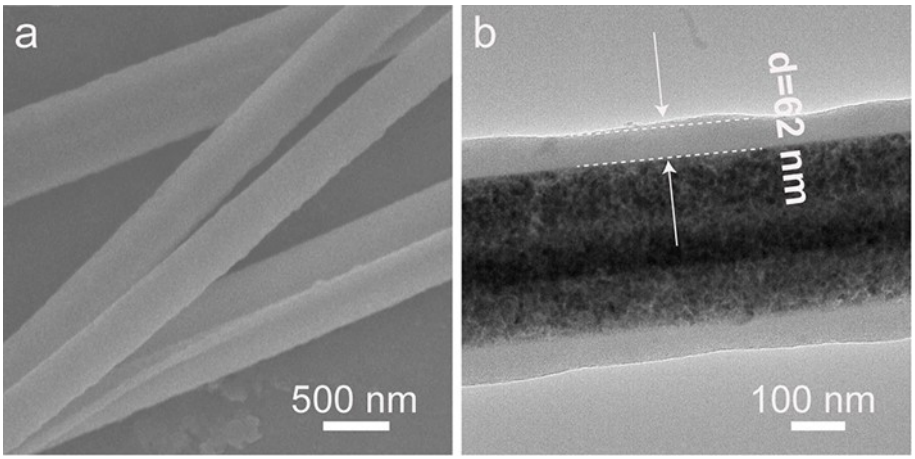

Fig. S5. (a) SEM image and (b) TEM image of Fe_3C-C@CTs nanowires.

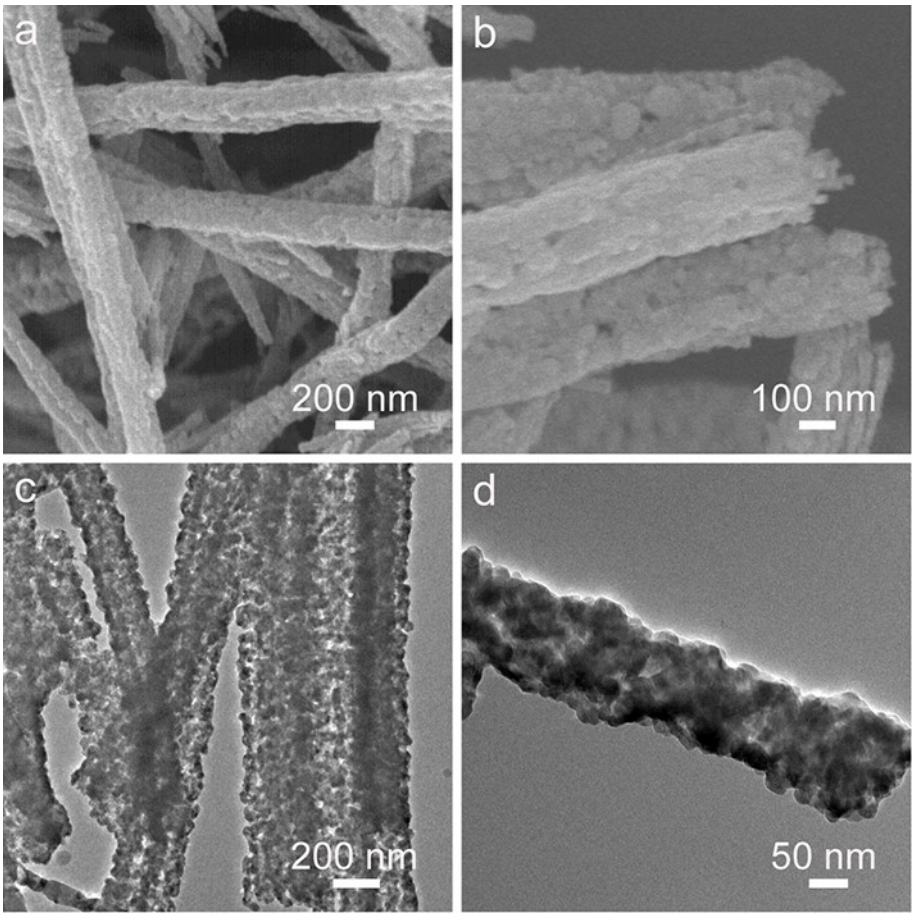

Fig. S6. (a, b) SEM images, (c, d) TEM image of FeS_2-C nanowires.

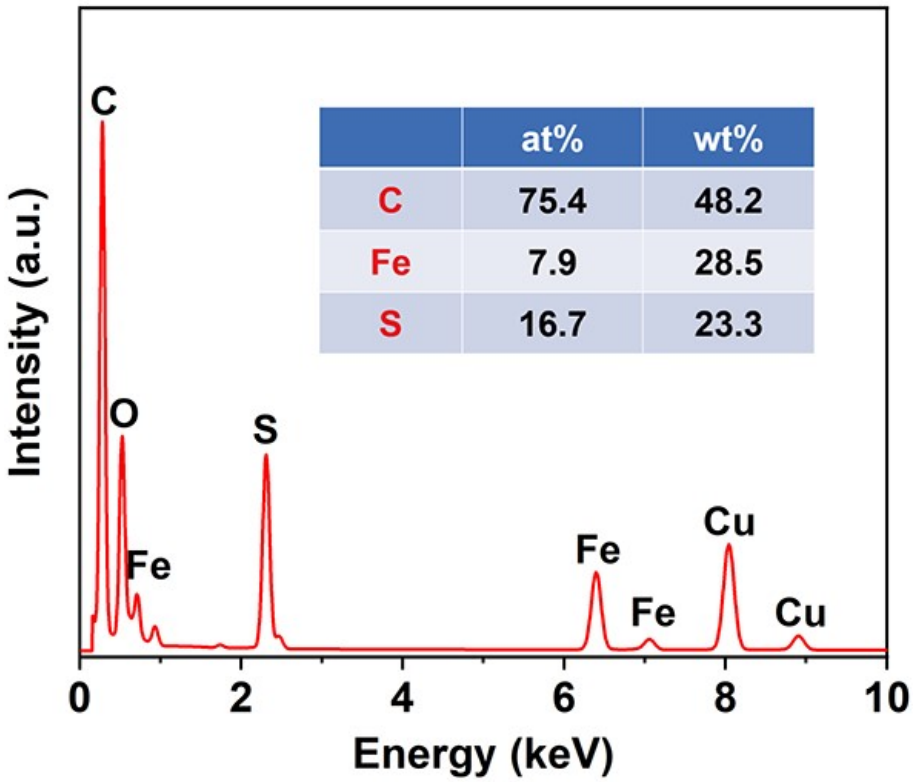

Fig. S7. EDX spectrum of uniformly FeS_2-C@CTs nanowires nanowires.

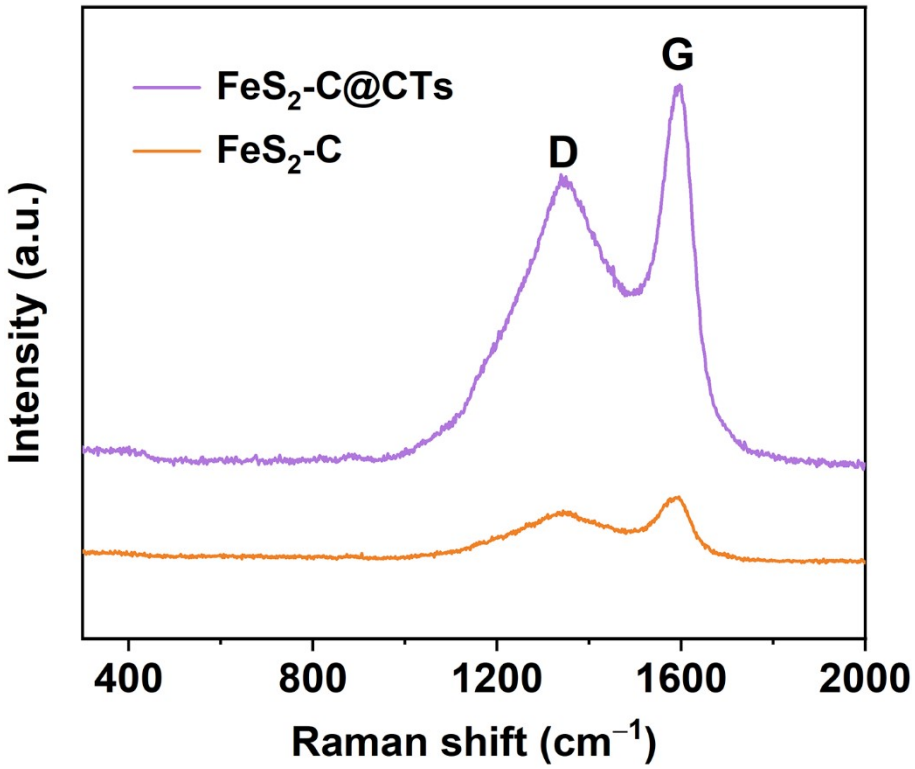

Fig. S8. Raman spectrum of the FeS_2-C@CTs and FeS_2-C nanowires.

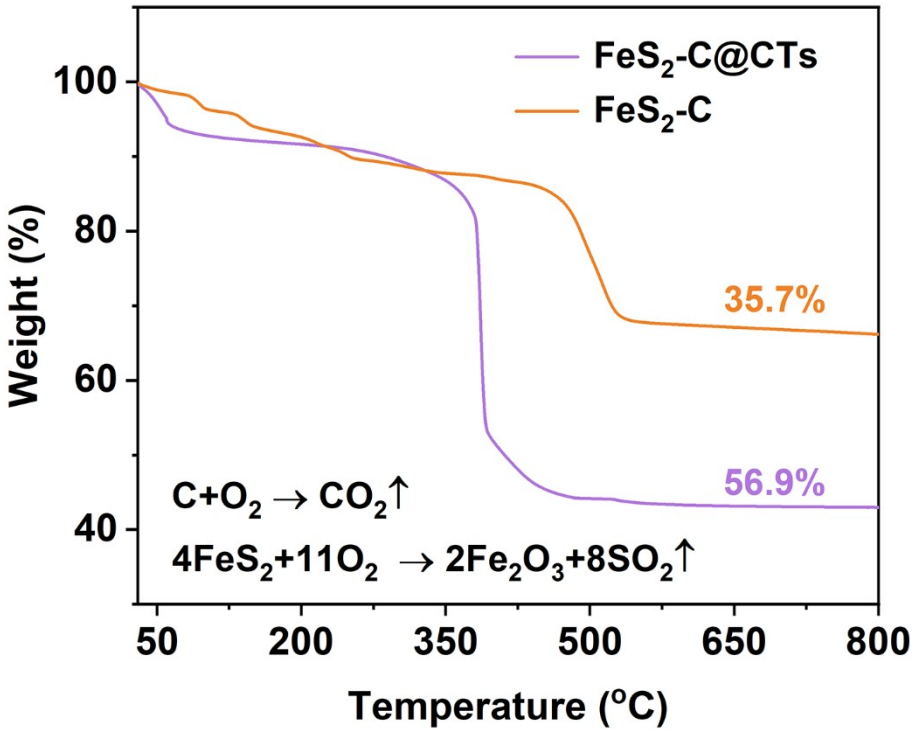

Fig. S9. TGA curves of FeS_2-C@CTs and FeS_2-C nanowires with a temperature ramp of 10 °C min^{-1} in an air atmosphere.

As shown in Fig. S8, the weight loss below 200 °C was mainly derived from the vaporization of adsorbed water, while the dramatic decline can be attributed to the decomposition of carbon and the conversion of FeS_2 into Fe_2O_3 after 200 °C. It was found that the mass of FeS_2-C@CTs and FeS_2-C nanowires decreased by 56.9% and 33.4% after annealing process, respectively. Taking FeS_2-C@CTs as an example, the content of carbon can be calculated according to the following equations:[1]

$CNTs/FeS_2@C \rightarrow Fe_2O_3 + gas$ atomic weight: Fe (56), S (32), O (16)

$$x + \frac{[(56 + 32 * 2) - (56 * 2 + 16 * 3)/2](1 - x)}{56 + 32 * 2} = 56.9\%$$

The total weight percentage of FeS_2-C@CTs is considered as 100%, while the carbon weight percentage is x. According to the above equation, the carbon content of FeS_2-C@CTs is calculated to be 35%. In the same way, the carbon content of FeS_2-C is calculated to be 4%.

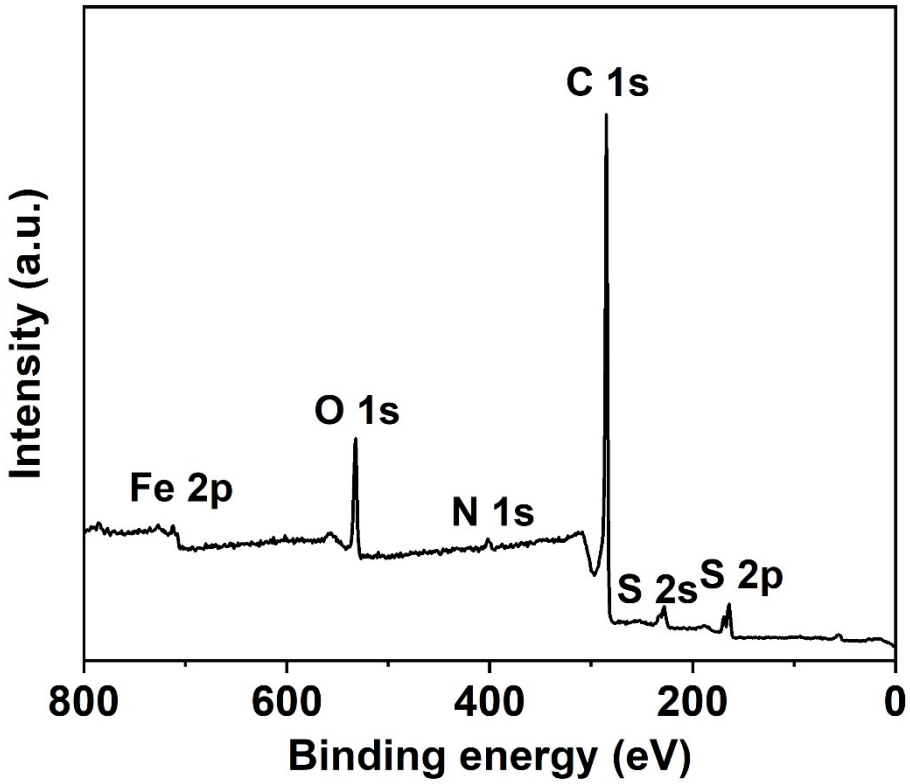

Fig. S10. XPS spectra of FeS_2-C@CTs nanowires.

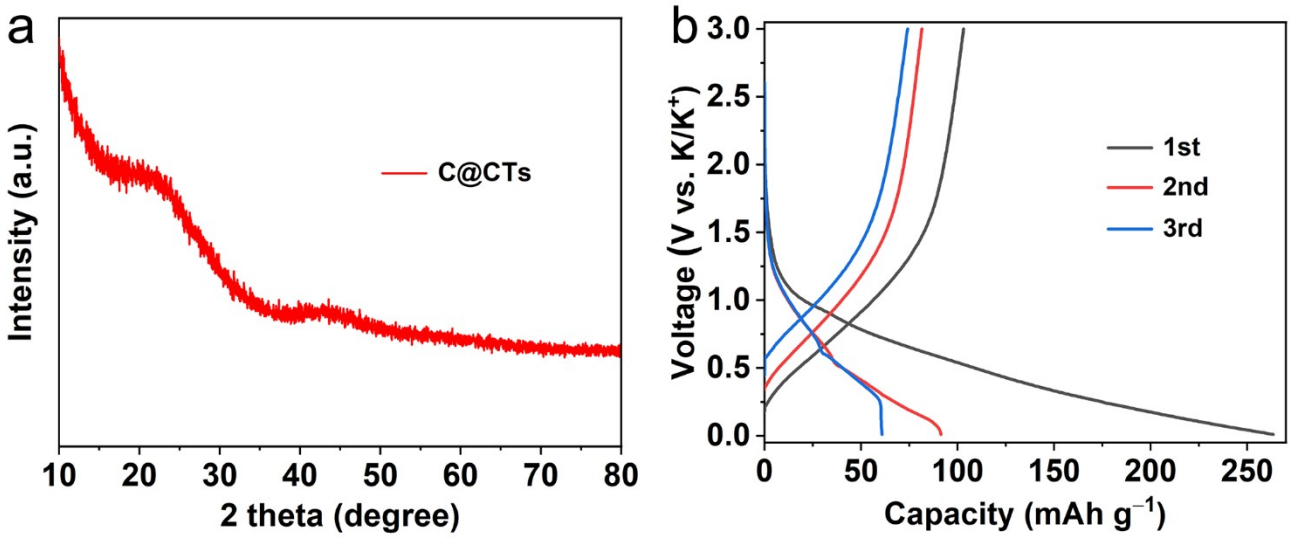

Fig. S11. (a) XRD pattern and (b) charge–discharge curves of C@CTs nanowires.

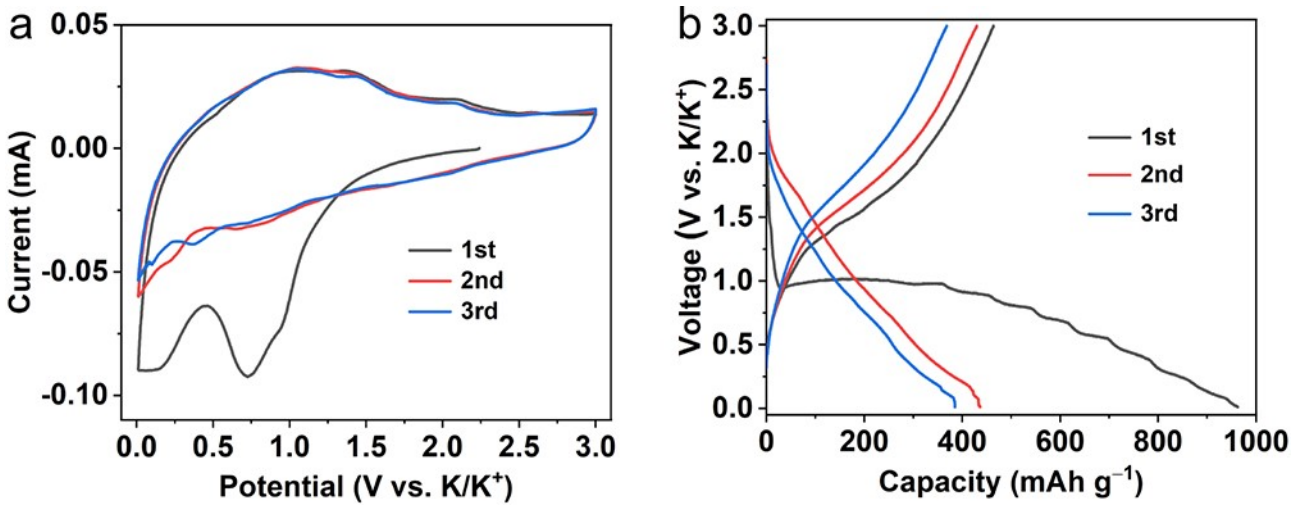

Fig. S12. (a) CV curves at 0.1 mV s^{-1} and (b) charge–discharge curves from 50 mA g^{-1} of FeS_2-C nanowires.

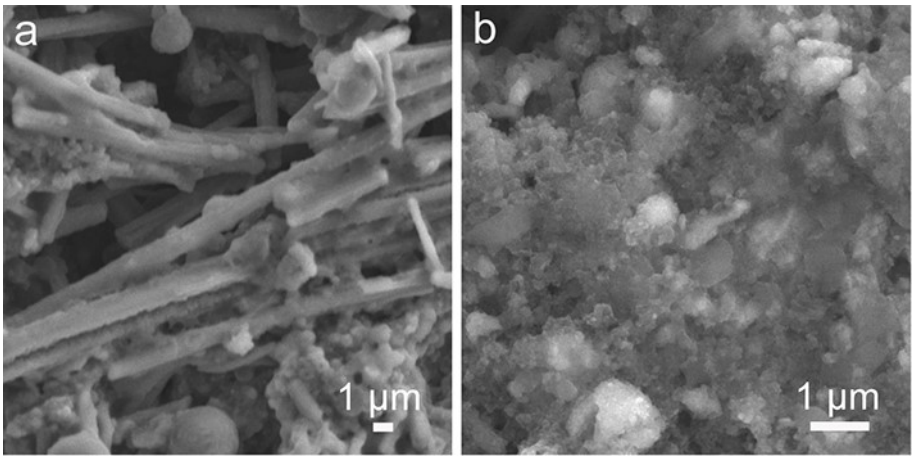

Fig. S13. (a) SEM image of the FeS_2-C@CTs electrode after 300 cycles. (b) SEM image of the FeS_2-C electrode after 300 cycles.

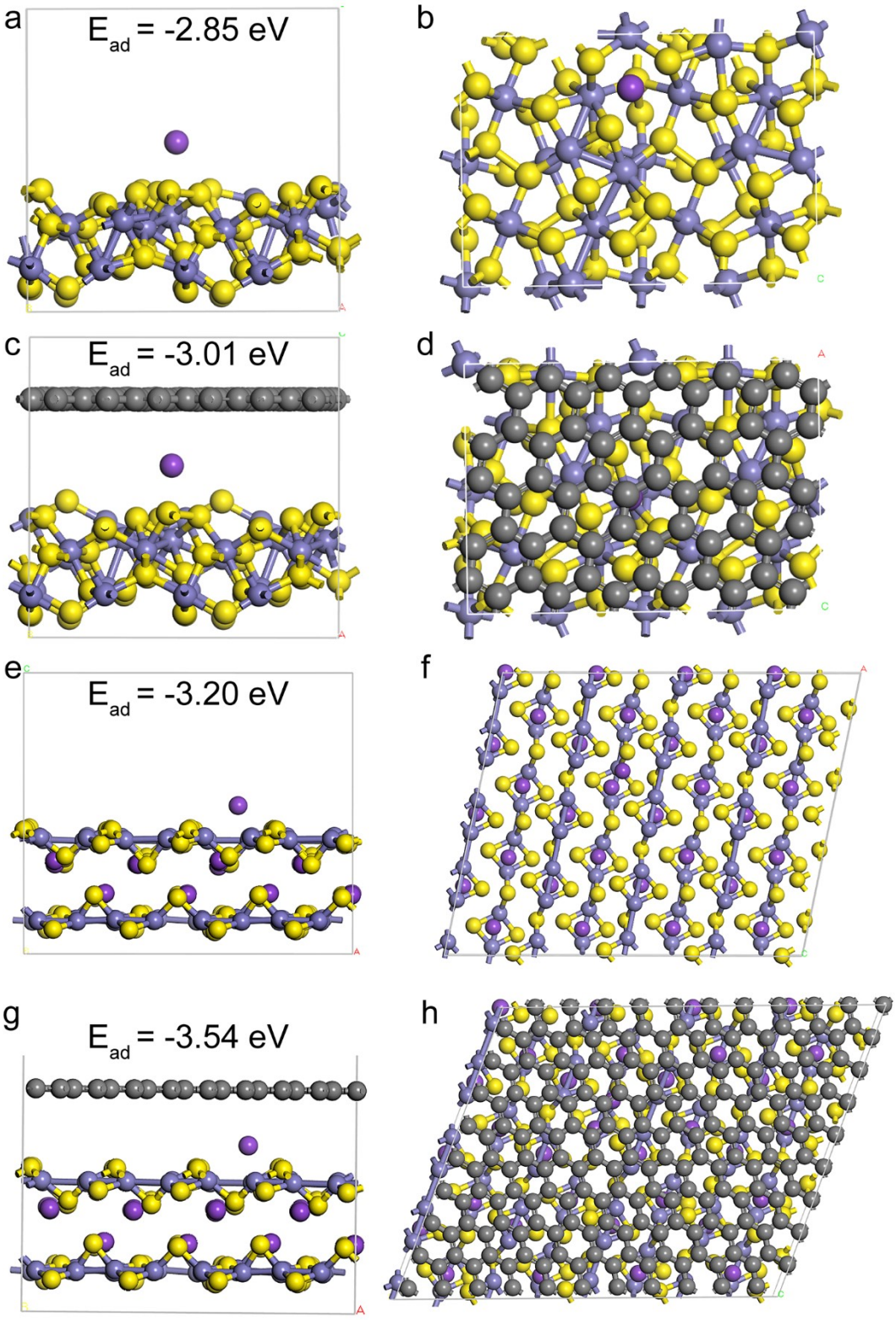

Fig. S14. Side and top views of the geometry structure with one K-ion absorbed on (a, b) FeS_2 surface, (c, d) FeS_2-C@CTs, (e, f) $KFeS_2$ surface and (g, h) $KFeS_2$-C@CTs.

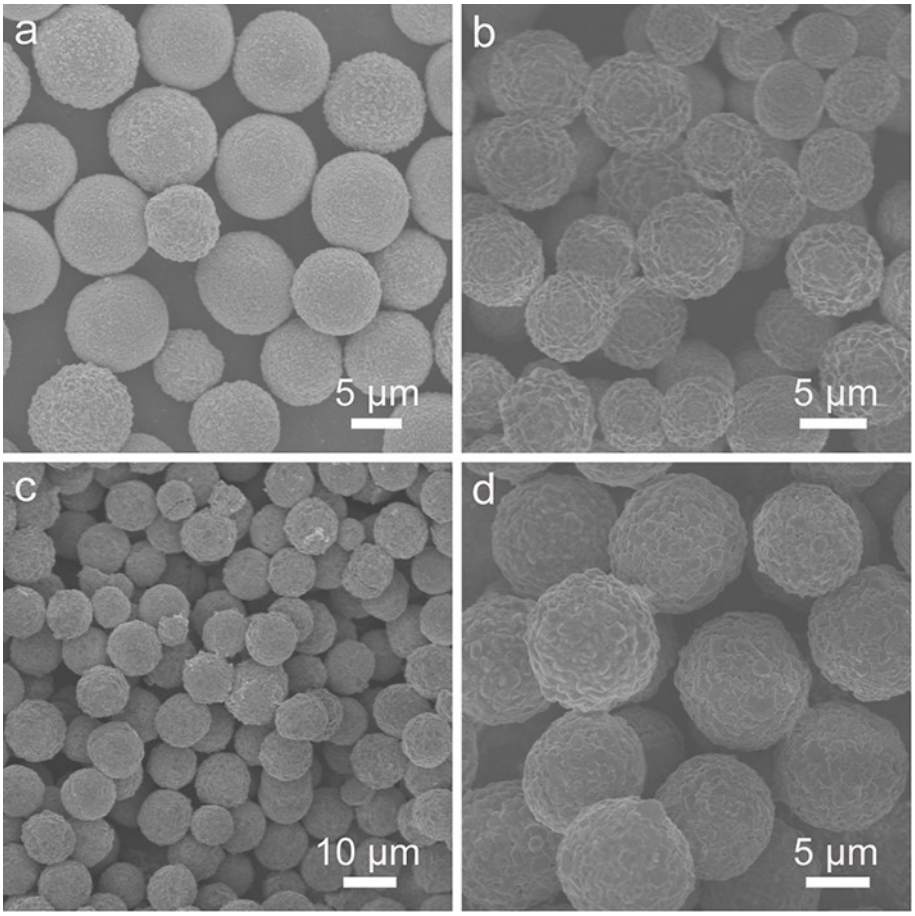

Fig. S15. (a) SEM image of $CoCO_3$ microspheres, (b) SEM image of Co_3O_4 microspheres, and (c,d) SEM images of P2-type $K_{0.6}CoO_2$ microspheres.

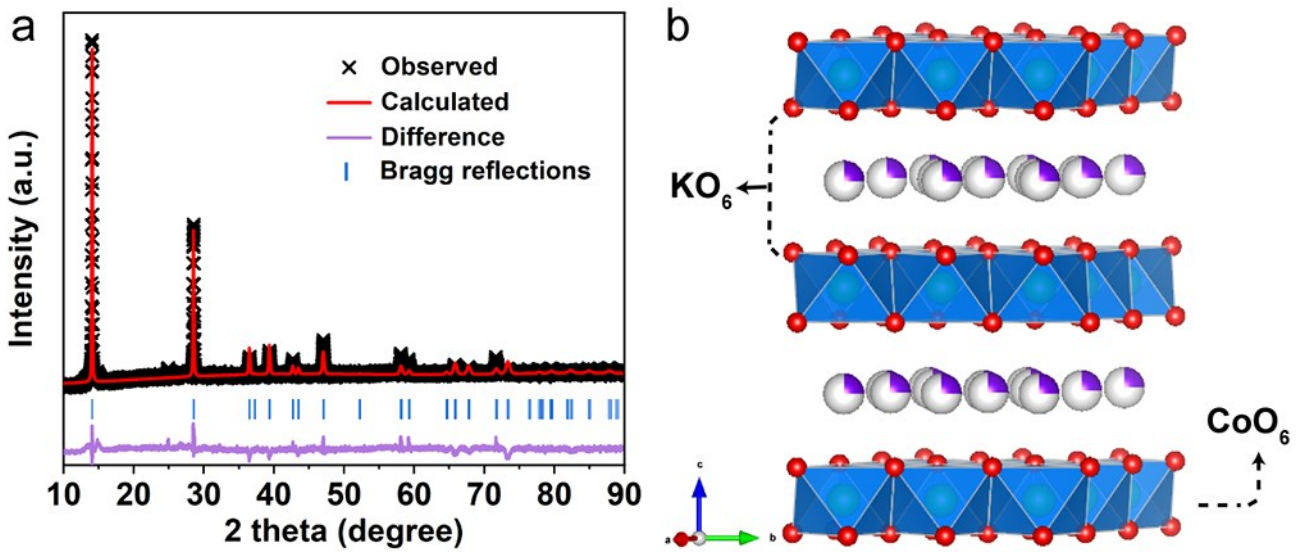

Fig. S16. (a) Rietveld refinement of X-ray diffraction data and (b) schematic structure of the P2-type $K_{0.6}CoO_2$ microspheres.

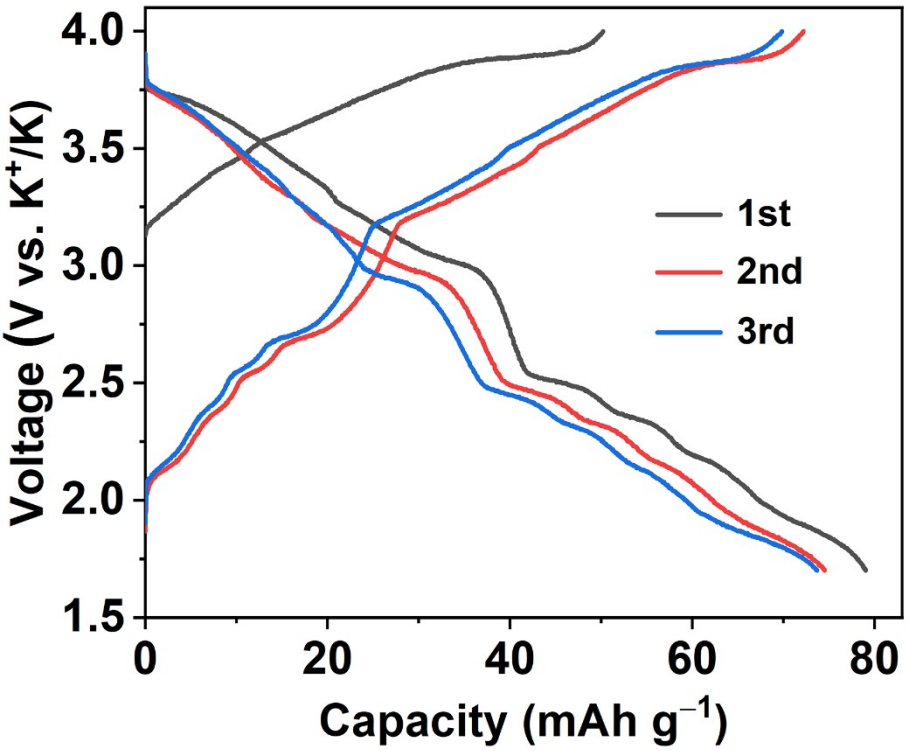

Fig. S17. Typical charge–discharge curves of $K_{0.6}CoO_2$.

Table S1. Comparison of properties of the FeS_2-C@CTs nanowires with the previously reported FeS_2-based anodes.

Materials	Reversible capacity (mAh g^{-1})	Cycling stability	Particle size (nm)	References
FeS_2-C@CTs	**524 (50 mA g^{-1})**	**82.3% (1000 cycles)**	**10**	**This work**
MCS-FeS_2@C-20	519 (50 mA g^{-1})	84% (500 cycles)	150	[2]
H-FeS_2@3DCS	516 (50 mA g^{-1})	≈100% (1000 cycles)	≤ 30	[3]
FeS_2@C nanoparticles	521 (500 mA g^{-1})	86% (100 cycles)	10	[4]
G@porousFeS_2@C composite	431 (300 mA g^{-1})	90% (30 cycles)	35	[5]
FeS_2@RGO-2	151 (500 mA g^{-1})	81% (420 cycles)	300	[6]
m-FeS_2@C-SSNFG	523 (50 mA g^{-1})	72% (1000 cycles)	20	[7]
Rod-like FeS_2/C@C	340 (100 mA g^{-1})	77% (100 cycles)	50	[8]
FeS_2@C nano-candied haws	495 (100 mA g^{-1})	73% (300 cycles)	500	[9]
FeS@NC nanosheets	415 (100 mA g^{-1})	69% (1100 cycles)	10~200	[10]
Fe_7Se_8@C nanotubes	344 (100 mA g^{-1})	89% (500 cycles)	~5	[11]
ZnS@C	336 (100 mA g^{-1})	115% (2300 cycles)	~20	[12]

Table S2. Comparison of electrochemical properties of the $K_{0.6}CoO_2$//FeS_2-C@CTs full battery and

other reported FeS_2-based potassium-ion full batteries.

Full cells	Reversible capacity (mAh g^{-1})	Cycling stability	Rate capability (mAh g^{-1})	References
$K_{0.6}CoO_2$//FeS_2-C@CTs	**230 (50 mA g^{-1})**	**88% (200 cycles)**	**125 (1 A g^{-1})**	**This work**
PTCDA//$Fe_{1-x}S$@C-3	330 (50 mA g^{-1})	37% (150 cycles)	165 (1 A g^{-1})	[13]
KCo_2O_4//FeS_2@C	146 (100 mA g^{-1})	78% (100 cycles)	53 (0.5 A g^{-1})	[9]
$K_{0.4}CoO_2$// MCS-FeS_2@C-20	239 (50 mA g^{-1})	86% (200 cycles)	69 (0.8 A g^{-1})	[2]

References

1 Y. Liu, Q. Deng, Y. Li, Y. Li, W. Zhong, J. Hu, X. Ji, C. Yang, Z. Lin, K. Huang, CoSe@N-Doped Carbon Nanotubes as a Potassium-Ion Battery Anode with High Initial Coulombic Efficiency and Superior Capacity Retention, *ACS Nano*, 2021, **15**, 1121–1132.

2 Z. Zhang, L. Duan, Y. Xu, C. Zhao, J. Bao, J. Shen, X. Zhou, Synthesis of multicore-shell FeS_2@C nanocapsules for stable potassium-ion batteries, *J. Energy Chem.*, 2022, **73**, 126–13.

3 Y. Cui, W. Feng, D. Wang, Y. Wang, W. Liu, H. Wang, Y. Jin, Y. Yan, H. Hu, M. Wu, Q. Xue, Z. Yan, W. Xing, Water-Soluble Salt Template-Assisted Anchor of Hollow FeS_2 Nanoparticle Inside 3D Carbon Skeleton to Achieve Fast Potassium-Ion Storage, *Adv. Energy Mater*., 2021, **11**, 2101343.

4 Y. Luo, M. Tao, J. Deng, R. Zhan, B. Guo, Q. Ma, M. Aslam, Y. Qi, M. Xu, Nanocubes composed of FeS_2@C nanoparticles as advanced anode materials for K-ion storage, *Inorg. Chem. Front.*, 2020, **7**, 394–401.

5 Q. Yao, J. Zhang, X. Shi, B. Deng, K. Hou, Y. Zhao, L. Guan, Rational synthesis of two-dimensional G@porous FeS_2@C composite as high-rate anode materials for sodium/potassium ion batteries, *Electrochim. Acta*, 2019, **307**, 118–128.

6 J. Xie, Y. Zhu, N. Zhuang, H. Lei, W. Zhu, Y. Fu, M.S. Javed, J. Li, W. Mai, Rational design of metal organic framework-derived FeS_2 hollow nanocages@reduced graphene oxide for K-ion

storage, *Nanoscale*, 2018, **10**, 17092–17098.

7 K. Han, W. Zhao, Q. Yu, Z. Liu, P. Li, W. Wang, L. Song, F. An, P. Cao, X. Qu, Marcasite-FeS_2@carbon nanodots anchored on 3D cell-like graphenic matrix for high-rate and ultrastable potassium ion storage, *J. Power Sources*, 2020, **469**, 228429.

8 X. Li, H. Wang, W. Zhang, Y. Feng, J. Ma, S-Doped Carbon-Coated FeS_2/C@C Nanorods for Potassium Storage, *Acta Metall. Sin.*, 2021, **34**, 321–328.

9 Y. Du, W. Weng, Z. Zhang, Y. He, J. Xu, J. Sun, J. Liao, J. Bao, X. Zhou, Candied-Haws-like Architecture Consisting of FeS_2@C Core-Shell Particles for Efficient Potassium Storage, *ACS Mater. Lett.*, 2021, **3**, 356–363.

10 J. Yuan, M. Mu, X. Xu, Y. Gan, H. He, X. Zhang, X. Li, F. Kuang, H. Li, J. Liu, Three-dimensional porous FeS@N doped carbon nanosheets for high-rate and high-stable sodium/potassium storage, *Compos. Part B-Eng.*, 2022, **247**, 110300.

11 J. Yuan, Y. Gan, X. Xu, M. Mu, H. He, X. Li, X. Zhang, J. Liu, Construction of Fe_7Se_8@Carbon nanotubes with enhanced sodium/potassium storage, *J. Colloid Interface Sci.*, 2022, **626**, 355–363.

12 X. Xu, D. Zhang, Z. Wang, S. Zuo, J. Yuan, R. Hu, J. Liu, Ultrafine ZnS Nanoparticles in the Nitrogen-Doped Carbon Matrix for Long-Life and High-Stable Potassium-Ion Batteries, *ACS Appl. Mater. Interfaces*, 2021, **13**, 11007–11017.

13 X. Shi, Y. Gan, Q. Zhang, C. Wang, Y. Zhao, L. Guan, W. Huang, A Partial Sulfuration Strategy Derived Multi-Yolk-Shell Structure for Ultra-Stable K/Na/Li-ion Storage, *Adv. Mater.*, 2021, **33**, 2100837.